Alexandria Engineering Journal

Deposition of sediment mixture due to jet effluent into a rectangular shallow reservoir

Sameh Ahmad Kantoush, Anton J. Schleiss
Ecole Polytechnique Fédérale de Lausanne (EPFL), Laboratory of Hydraulic Constructions (LCH),CH-1015 Lausanne, Switzerland
Hossam Nagy
Faculty of Eng., Alexandria University, Alexandria, Egypt

With the purpose of controlling the sedimentation in shallow reservoirs, the effects of the geometry on flow pattern and deposition processes were investigated with systematic physical experiments and numerical simulations. This allowed identifying ideal off-stream reservoir geometries, which can minimize or maximize the settlement of suspended sediments. The objective is also to gain deeper insight into the physical processes of sedimentation in shallow reservoirs governed by suspended sediments. The experimental investigation of the flow and sediment behavior in axi-symmetric geometries with different shapes provides further information on the evolution of the flow pattern and the sediment deposition. Beside the expansion ratio and form ratio of the basin, the flow regime was classified by the geometry shape factor SK and inlet Froude number Fr_{in}. Empirical relationships for the estimation of the reattachment length of gyres and the normalized residence time as a function of the geometry shape factor, SK, were established. The numerical simulation revealed that the observed asymmetry in flow and deposition patterns can be explained by the sensitivity of the flow regarding geometry and boundary conditions. Recommendations are given for the design procedure of a new shallow reservoir in view of minimizing the sedimentation due to suspended sediment. The deposited sediment volume can be efficiently minimized by optimal designed reservoir geometry.

الهدف من هذه الدراسة هو فهم وتحليل للعمليات الطبيعية وآلية الترسيب فى الخزانات الضحلة التى تحمل مياهها كميات من الترسيبات المعلقة. وقد تم بحث سبل التحكم فى ظاهرة الترسيب فى الخزانات العميقة عن طريق تغيير الشكل الهندسى للخزان، وذلك باجراء تجارب معملية ونمذجة عددية باستخدام الحاسب الآلى تحاكى ما يحدث فى الطبيعة. ومن نتائج هذه الدراسة أنها ساهمت فى تحديد وتعريف الشكل المثالى للخزانات التى تسمح بترسيب أقل أو أكبر كمية من الترسيبات. وقد نتج من الدراسات المعملية إستحداث متغيرين غير بعديين ومؤثرين فى حركة الجريان وحركة الترسيبات وهما معامل الشكل ورقم فرود للمدخل. ومعامل الشكل يعتبر دالة فى المحيط المبلل ومساحة سطح الخزان ونسبة الطول الى العرض ونسبة الإتساع للمدخل. وقد تم إستنتاج معادلات وضعية لتوصيف شكل الجريان فى الخزان وتقدير الأطوال اللازمة وزمن بقاء المياه بالخزان. وكذلك تم إستنتاج معادلات وضعية لنوعية الجريان المندفع وسرعته. وكذلك تم عمل معادلة وضعية لحساب دليل الترسيب، وكفائة اصطياد الترسيبات وسمك الطبقة الترسيبات. وقد قدمت الرسالة توصيات للحصول على الشكل الهندسى الأمثل للخزان الضحل لتقليل الترسيبات نتيجة للرمال المعلقة بالمياه.

Keywords: Shallow flow, geometry shape factor, reservoir geometry, turbulent jet, flow and sediment deposition patterns, suspended sediments, reservoir sedimentation,

1. Introduction

1.1. Background

Lakes, reservoirs, bays, estuaries as well as coastal regions often have a very shallow bathymetry. Vertically mixed flows in these systems may be forced by wind shear, by tidal action, by breakdown of yet larger scale inertial currents, and by river inflows. Shallow flows are bounded, layered turbulent flows in a domain for which 2D, namely the flow and the transversal dimensions, greatly exceed the vertical one.

The present study particularly focuses on shallow reservoirs with a prototype depth between 5.0 and 15.0 m and mainly governed by suspended sediments. Recent laboratory experiments and numerical simulations for a wide flume (Sloff et al., 2004) showed that

channel formation in shallow reservoirs is controlled by the flow pattern. Experimental investigation on the silting process in reservoirs and lakes was carried out systematically by (Mertens, 1985) in a square, shallow basin (5.00 × 5.00 × 0.25 m) with a horizontal bottom.

The silting-up of reservoirs is a very complex process. Shear flow over a mobile bed induces sediment transport and the generation of bed forms. The interaction between the flow and the bed usually produces different types of regular patterns characterized by a wide range of sizes and shapes (dunes, ripples, anti-dunes, etc.). In turn, both sediment transport and bed forms, influence the flow. The importance of studying the presence and evolution of these regular patterns arises because those bed forms generated by the sediment transport can increase the resistance to flow. In particular, experimental results on the influence of suspended sediment on turbulence are still lacking.

1.2. Aim of the study

This study focuses on the sedimentation of shallow reservoirs by suspended sediments and the objective of the experiments is to gain insight into the physical process behind the sedimentation of shallow reservoirs governed by suspended sediment. Moreover, it is aiming at a better understanding of the mechanism governing the sediment exchange process between the jet entering the reservoir and the associated turbulence structures. Furthermore, we would like to examine different test procedures and find the optimal one to continue with future test configurations. These experiments are part of test series prepared to investigate the ideal reservoir geometry, minimizing the settlement of suspended sediments. The experiment described hereafter is expected to fill in part of our knowledge gap.

2. Experimental setup

2.1. Similarity and dimensions

Comprehensive information on similitude requirements for movable and fixed bed models can be found in Yalin, 1970 and Kobus, 1980. Scaled physical models are based on similarity theory, which uses a series of dimensionless parameters that fully or at least partially characterize the physics. The choice of a scaling factor $\lambda=L_p/L_m$, or length scale ratio, to be used in the experiments, is determined by the objectives of the research. According to the length of the tested section and the laboratory constraints, the model has been designed with horizontal and vertical scales of $\lambda_l = \lambda_h = 50$ (Kantoush et al., 2005). Application of the above similarity rules is shown in table 1, with a comparison between the prototype and the model characteristic values.

The experiments were carried out in a specially built facility at the Laboratory of the Hydraulic Constriction (LCH) of Federal Institute of Lausanne (EPFL). The dimensions of the model were based on those of the Rhône River and the space available in the laboratory. A schematic view of the experimental setup is shown in Fig. 1. The setup consists of an inlet rectangular channel 0.25 m wide and 1.0 m long made of PVC, a rectangular shallow basin with inner dimensions of 6.00 m length and 4.00 m width, an outlet rectangular channel 0.25 m wide and 1.0 m long, a flap gate 0.25 m wide and 0.30 m height at the end of the outlet (to control the water level), a drainage pipe 0.23 m diameter fixed after the flap gate, and stilling basin to collect the sediment and drainage the water in see fig. 1.

The bottom and the walls of the basin consist of 8 mm thick PVC plates with 0.30 m height on the sides. Adjacent to the experimental reservoir, a mixing tank with a maximum capacity of 200 liters is used to prepare and store the sediment fluid mixture. A sediment supplier tank is mounted above the mixing tank. To control the sediment concentration, a small gate is installed at the down front of the sediment tank. Sediment supplier tank is attached to a vibrator, which has several speeds to increase or decrease the sediment concentrations. The mixing tank is equipped with a propeller type mixer to create a homogenous sediment concentration. After filling the experimental reservoir with water, the water-sediment mixture will flow by gravity into the rectangular basin through a flexible pipe with 0.10 m diameter. To ensure a uniform mixture in the mixing tank and reservoir basin, the density of the sediment mixture and the clear water were controlled before and dur-

ing the experiments by means of a turbidity meter. On the basin side walls a movable aluminium frame is mounted with 4.0 m length, which carries the measurement instruments can move in three directions. The parameters that were measured during the experimental runs are shown at table 2.

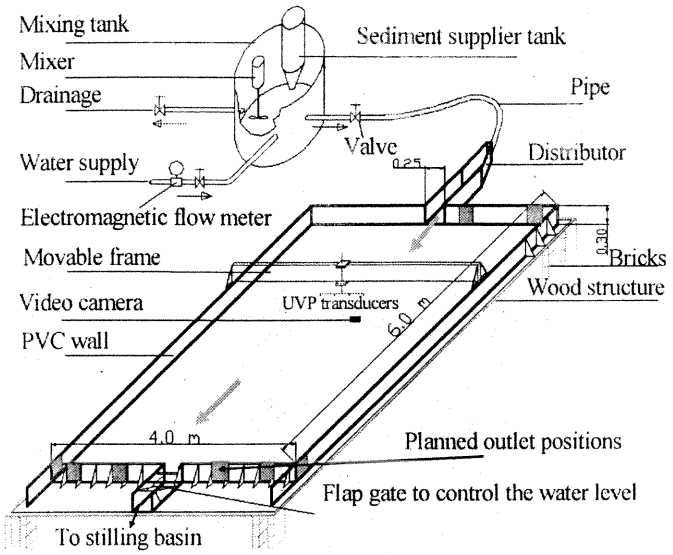

Fig. 1. Schematic drawing of the experimental installation.

Table 1
Characteristic values of the prototype and the model (scale 1:50)

Item	Prototype	Model
Length, L[m]	300.0	6.0
Width, B[m]	200.0	4.0
Water depth, h[m]	7.6-15.2	0.20
Discharge, Q [m^3/s]	5.0	0.007
Median grain size, d_{50}[mm]	0.037	0.05
Sediment concentration, Cs [g/l]	5.0	3.0
Gradient of section, I [-]	1.0%	0.0%

Table 2
Model parameters and instrumentation

Measured parameters	Dimension	Instrument
Water level	[m]	Ultrasonic probe
Sediment thickness	[m]	Echo sounder
Discharge	[m^3/s]	Flow meter
Surface velocity	[m/s]	PIV technique
Sediment concentration	[g/l]	Turbidity meter
Temperature	[C°]	Thermistors

2.2. Experimental conditions

To model suspended sediment currents in the laboratory model, walnut crushed shells with a median grain size d_{50}=50μm, density 1500 kg/m^3 was used in all tests cases. These are non cohesive, light weight and homogeneous grain material. The sediments are added to the mixing tank during the tests. The hydraulic conditions were chosen to fulfill the sediment transport requirements see Error! Reference source not found.. Furthermore, for all test cases, Froude number is small enough and Reynolds number is high enough to ensure subcritical fully developed turbulent flow.

2.3. Measurements and data acquisition system

Several parameters were measured during every test; namely: surface velocities, deposited sediment layer thickness, suspended sediment concentration at the outlet, 3D flow velocity, water level and water temperature. Table 2 provides an overview of the measurements and instrumentations used during the tests.

The velocities were measured by means of an Ultrasonic Doppler Velocity Profiler, which allows an instantaneous measurement of the 1D velocity profile over the whole flow depth (Metflow, 2002). The measurement probes were mounted on a support in groups of three, allowing the measurement of the 3D flow field fig. 2. To cover the whole cross section of the basin, 5 positions were chosen along the cross section; each position has four groups of three probes. All twelve probes were mounted on a frame which moves in the two horizontal directions. The probes were inclined at 20° to the vertical and had an emitting frequency of 2 MHz. The velocity measurements were taken at about 480 measurement points.

The bed level development was measured by means of Miniature echo sounder (UWS) see table 3. The transmitted ultrasound impulse is reflected at any object serving as a target. This acoustic reflection (echo) propagates in space and is received from the ultrasound sensor. In order to measure the effective distance between target and sensor the run-time must be determined which the sound needs from the sensor to the target and back

needs from the sensor to the target and back to the sensor again. The measured run-time will be averaged. The distance to the target in meters can be calculated by the run-time and the sound velocity. The UWS was mounted on the movable frame fig. 4 to scan the whole basin area (6m*4m). The measured cross sections profiles were spaced at 0.05 m and some case 0.025 m was tested, starting from 0.10 m from the model's side wall, and ending at 0.10 m from the other wall, i.e. covering a total model width of 4.0 m with total 77 points. The measured longitudinal profiles were spaced at 0.20 and some case 0.1 was tested, starting from 0.05 m from the upstream sidewall, and ending at 0.10 m from the other downstream wall.

PIV offers a simple method of measurement in areas with complicated geometry and flow conditions. Surface flow measurements with PIV are described for e.g. in (Adrian, 1991). In hydraulic engineering, however, this technique has so far mainly been applied for surface velocity measurements of water and ice flow in very uniform flow fields as well as in groyne field experiments (Ettema et al., 1997; Fujita et al., 1998; Weitbrecht et al., 2002).

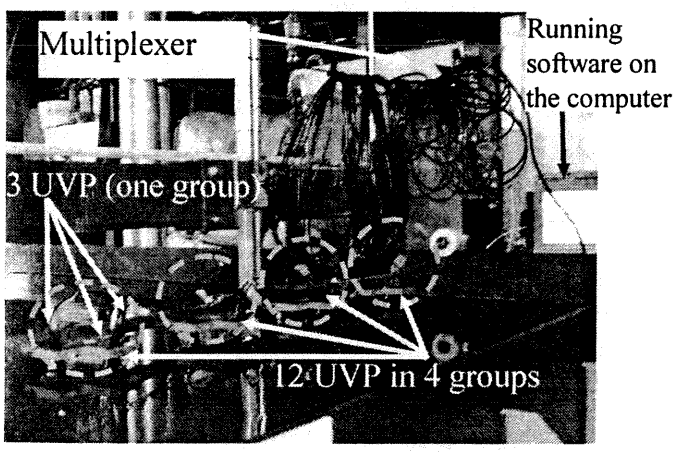

Fig. 2. Scheme of UVP installations and data acquisition.

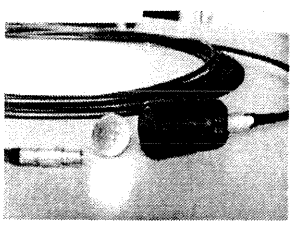

Fig. 3-a. Lab sensor.

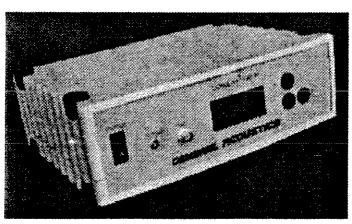

Fig. 3-b. Lab device UWS.

Table 3
Miniature echo sounder UltraLab UWS specifications

Specification
Lab device ULTRALAB UWS see fig. 3-b
Control keys and integrated 4 digit 12mm LCD-Display
Dimensions: 330/115/260 mm, length/height/depth
Measuring rate: max. 10 Hz
Sensor see fig. 3-a
Dimensions: Diameter: 30mm/
Length: 50mm
Frequency: 1 MHz
Resolution: 1 % of measuring range, max. 1 mm
Accuracy: 1% of measured value at constant circumstances

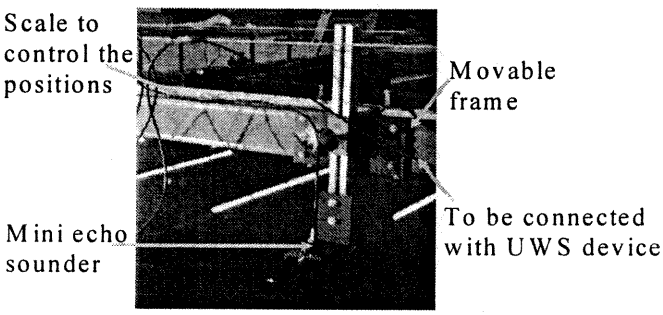

Fig. 4. Miniature echo sounder mounted on the frame.

The basic principal of PIV is simple: the flow is seeded with plastic particles (with average diameter 3.4 mm and specific weight 960.0 kg/m^3) which are then illuminated and their positions recorded at two successive instant.

Fig. 5 by video (SMX-155, monochrome, 1.3 megapixel, CMOS camera with USB2.0 interface and frame rate up to 33 FPS). The video of the whole 2D field is then divided into a number of interrogation areas and, in each area, the distance moved by the tracer particles from the time of the first image being recorded to the second is determined. Knowing the distance traveled and the time taken, the velocity of the flow in that area is therefore measured. This is done for every area, giving the 2D map of the instantaneous velocity field at the time of the recording. The camera fixed perpendicular on the basin covering the plane basin area (the whole width 4.0 m and 5.0 from the length, missing 0.5m from upstream and downstream ends). The displacement of the plastic particle images over the time between the exposure of the first frame and the second analyzed by FlowManager software.

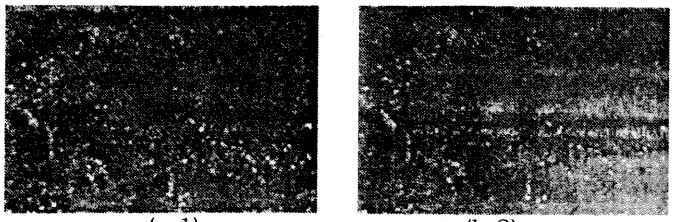

(a-1) (b-2)

Fig. 5. Typical PIV image pair.

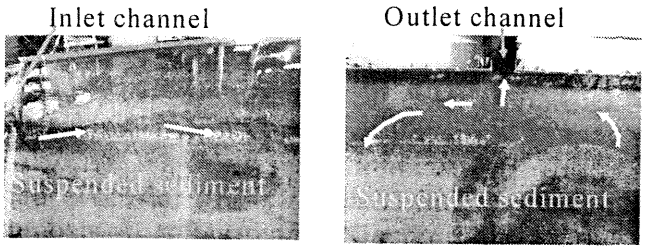

Fig. 6. Left: mixture entering; Right: mixture exit..

2.4. Test procedure

Two different experimental procedures were tested in order to find one approach for all test configurations. For this reason only experimental procedure for carrying out a standard continuously fed suspended sediment experiment will be described. The difference between the two procedures is as follows:
1. Discontinuous feeding: after 1hour of feeding sediment to the water mixture and doing the measurements (UVP, PIV and Pictures); close downstream flap gate, open water bypass and stop sediment feeding. After suspended sediment deposits, start bed level profile measurements as explained before.
2. Continuous feeding: working the whole duration continuously feeding the mixture and doing the measurements.

Prior to each experiment, the mixing tank and the basin were cleaned. The pump was started and the electromagnetic flow meter and a valve were then used to adjust the desired inflow rate. The down-stream flap gate was regulated according to the ultra sound calibration curve to control the water level. Then the basin and mixing tank were filled with clear water. One hour after starting the pump and stabilizing the flow, the PIV measurements were performed for that initial case (only clear water entering the basin). Sediment was added to the sediment supplier tank and the sediment concentration which enters the mixing tank was checked. The mixer guaranteed a homogenous mixture in the tank. Fig. 6 shows the homogenous suspended sediment mixture. The left panel shows the sediment entering from the upstream inlet channel to the basin whereas the right one shows the mixture arriving at the outlet in a completely mixed state and a certain concentration flowed from the outlet channel.

UVP probes were mounted to start 3D velocities measurements. The bed profile was measured for specific chosen cross sections every 20 minutes. PIV measurements were repeated during the test every 30 minutes and attention was paid to the transitional case during the test (decided according to the surface velocity observations). All the runs were repeatedly recorded with a digital video camera for selected durations in order to track the changes in flow patterns, and to determine the propagation of the suspended sediment concentration. The experiment was then run until equilibrium conditions were reached, defined as a minimal change in water surface and bed slope over the two consecutive measurements. Equilibrium was usually achieved within 4.5 hours after starting the experiments. The flap gate was then closed to permit for the suspended sediment to deposit and then measuring of deposit thickness was started using UWS as explained above. Finally the sediment at the outlet basin was collected, dried and weighted to calculate the trap efficiency coefficient and sediment volumes as well.

2.5. Test series

Three different test series have been carried out with the same boundary conditions and initial conditions as explained before but with different test procedure as following:
1. Series 1: The discontinuous feeding procedure has been used.
2. Series 2: Repeated test for Series A, with the purpose to check the reproducibility and the model sensitivity.
3. Series 3: The continuous feeding procedure has been used with the same condition as previous series.

3. Results and discussions

3.1. Flow patterns

Averaged flow fields have been obtained by using Particle Image Velocimetry (PIV) techniques and are depicted in figs. 7 to 9, each figure contains five flow patterns as following:
a- Flow pattern for the initial state (no sediment neither in the basin nor in the mixing tank)
b- Flow pattern after 1.5 hour of adding sediment concentration in the mixing tank.
c- Flow pattern after 3 hours from the start with a constant sediment concentration.
d- Flow pattern after 4.5 hours from the beginning.
e- Flow pattern using a clear water inflow after completely stopping the sediment supply.

Figs. 7-a, 8-a and 9-a show that the flow enters as a plane jet issuing from the narrow leading channel to the wide basin. After jet issuance, the main flow tends towards the right hand side, generating a large and stable main gyre rotating anticlockwise and two small 'triangular' gyres rotating clockwise in the two upstream corners of the basin. The jet appears to be attracted to one of the side-walls. Its preference for the right side is weak since a stable mirror image of the flow pattern can easily be established by slightly adapting the initial conditions. By following floating particles, it is noticed that in the first meter from the entrance the particle is straightly entering and, in the next two meters, it deflects to the right until it arrives at the stagnation points near the right wall at the middle (3m from the entrance). The particles that do not leave the basin through the outlet channel circulate with the main gyre to arrive near the separation zone at the farthest left side wall. There, a small gyre has formed at the left corner of the basin with a triangular shape 1.2m*1.2m. The circulation pattern sustains itself because the inertia of the main gyre pushes the in-coming jet aside. A bottom that is initially smooth favors this inertia dominated pattern. By comparing the three figures similar gyre patterns are obtained even with different test procedures and different working days.

The water-sediment mixture flows from the narrow inlet channel to the much wider basin. At first, the inflow mixture behaves like a jet that remains quite separated from the clear water in the basin. After some distance, the shear between both bodies of water moving at a different speed causes mass and momentum exchange and thus eddies that are peeled off from the core of the jet. This peeling off occurs alternatively on both sides of the jet and generates eddies that increase with longitudinal distance. Furthermore, the jet starts to undulate with a wavelength and amplitude that increase with longitudinal distance. The behavior resembles to a continuously growing instability. This asymmetric and switching flow behavior continues until the downstream end of the reservoir, where the jet is forced to pass through the outlet channel.

During 1.5 hours of adding the sediment the observed flow pattern in figs. 7-b, 8-b and 9-b did not differ much from what is previously explained for Series (a), except for the increase in size of the right corner gyre and a downstream shifted re-attachment point. Apparently this is due to the suspended sediment entrainment and the associated emergence of bed forms see fig. 10. It's clear that the flow structures in the different test series show a similar pattern in these figures.

Figs. 7-c, 8-c and 9-c present the flow patterns after 3 hours of adding sediment for the three test procedures. As a result of ripple formation and suspended sediment concentrations the flow field is completely changed. The gyres in the upstream corners are suppressed if not disappeared and a pattern has emerged that is rather symmetric with respect to the center line. It is also seen that the remaining two gyres interact with the jet which shows some tendency to meander. Since the exchange with the upstream corners of the basin is very small, it is expected that not much deposition takes place in those areas. Apparently the changes in the bed forms or effective roughness resulting from the sediment deposition are capable of completely changing the overall flow pattern. Through the same mechanism a further development can be expected. By comparing the three figures it can be concluded that similar flow patterns have developed but with small differences regarding the dimensions and strength of the circulation cells. In particular with the continuous feeding experiment fig. 9-c, the asymmetry leading to the subsequent pattern can already be seen.

Figs. 7-d, 8-d and 9-d show the flow patterns that have developed after 4.5 hours of adding sediment for the different test procedures. Figs. 7-d and 8-d still show symmetric flow patterns with two gyres coupled to the jet flow. It is noticed that two very weak gyres that might have become laminar or stagnant have hardly any exchange with the main motion. In both figures the same test procedures were used which resulted in virtually identical flow patterns. Fig. 9-d presents the flow pattern of the continuous test procedure after 4.5 hours of adding sediment. It has a flow structure different from those in figs. 7-d and 8-d. Due to the continuous feeding procedure already during the third hour the right side gyre starts to enlarge in size and develops into the one shown in fig. 9-d. This pattern appears to be rather stable. With the help of bed evolution measurements and final bed deformation pictures, it can be said that during the transition zone from the initial counterclockwise gyre to the final clockwise gyre the roughness of the bed showed strong local variations. It should be mentioned that all the flow patterns shown in the figs. d remained during the subsequent 2.5 hours of observation.

Figs. 7-e, 8-e and 9-e present the flow patterns for the three test procedures after stopping the flow, clear water (without sediment) has been injected into the basin to investigate the further evolution of the bed at different time periods. The flow patterns in figs. 7-e and 8-e are similar and equal to the pattern of fig. 9-e. After restarting the flow it chooses the easiest path from the inflow to the outflow gate along the left side wall. The sedimentation from the previous period has apparently become too much of an obstacle to result again in a symmetric flow pattern. It shows at least that the symmetric flow pattern is not a very stable one and that in the long run it would have changed into one of the more stable asymmetric patterns anyhow.

3.2. Morphological development

This section presents a comparison of all test series for the time evolution of the bed. Figs. 10 to 12 present a detailed comparison of final bed elevation, 3D for sediment thickness layer after 4.5 hour and the contours of deposition patterns. For all the tested scenarios,

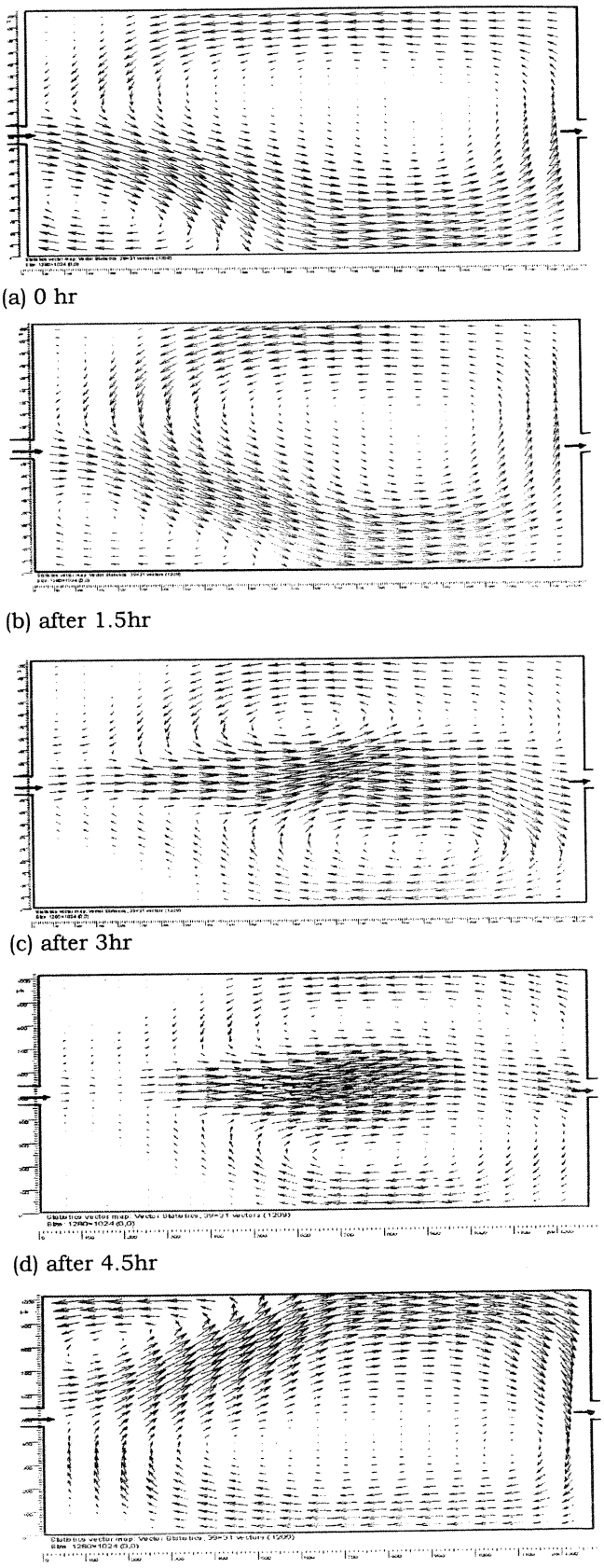

(a) 0 hr

(b) after 1.5hr

(c) after 3hr

(d) after 4.5hr

(e) clear water

Fig. 7. Flow pattern at different run times during test Series 1.

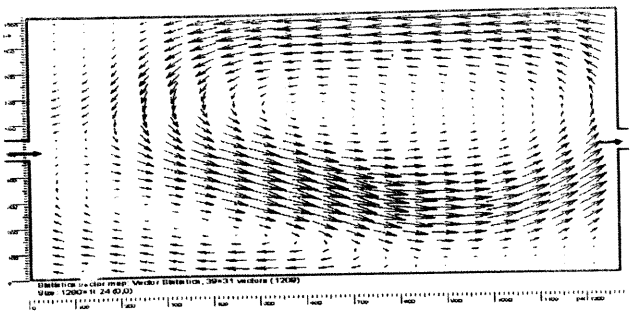

(a) 0hr

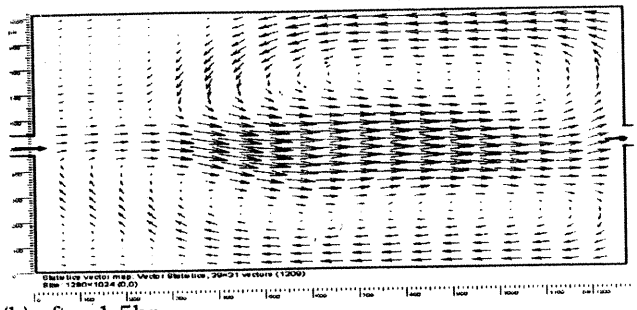

(b) after 1.5hr

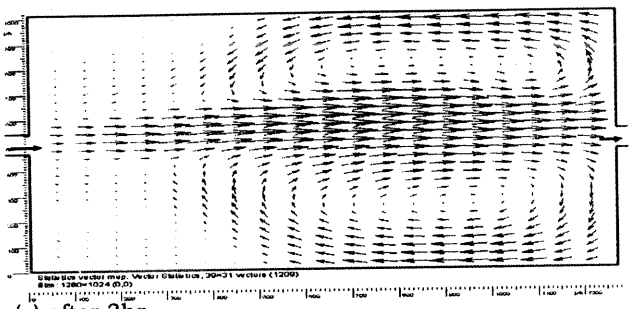

(c) after 3hr

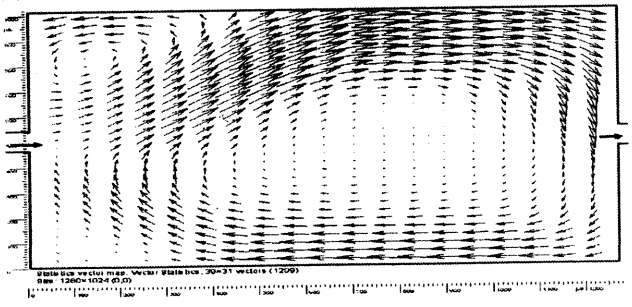

(d) 4.5hr

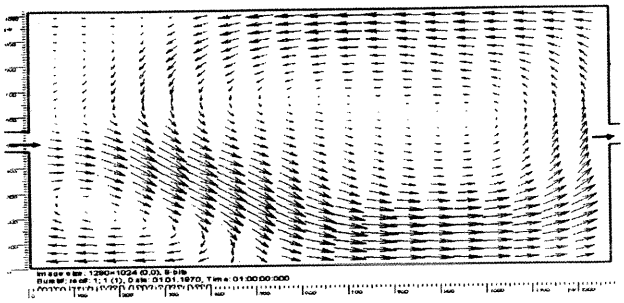

(e) clear water

Fig. 8. Flow pattern at different run times during test Series 2.

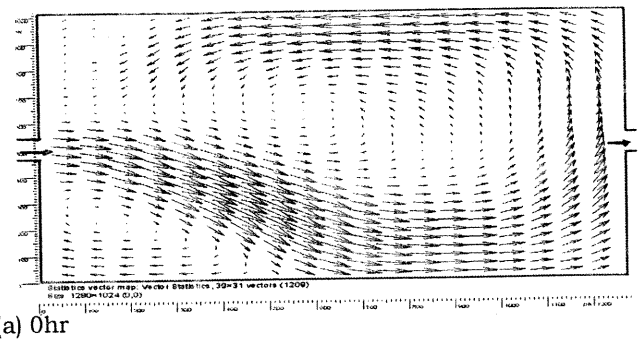

(a) 0hr

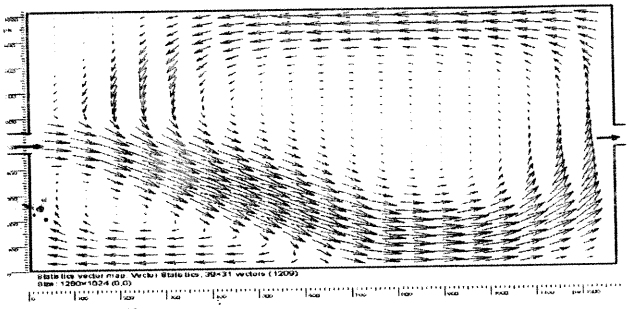

(b) after 1.5hr

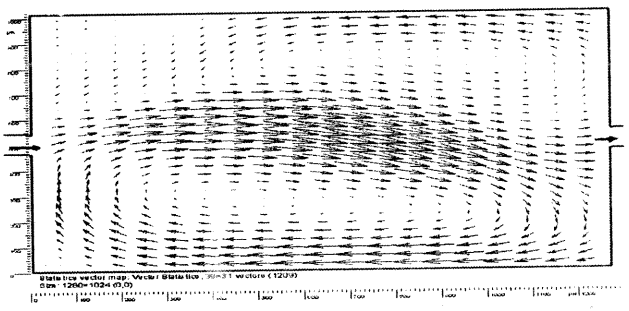

(c) after 3hr

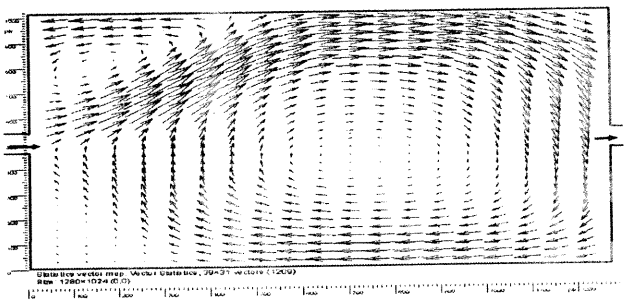

(d) after 4.5hr

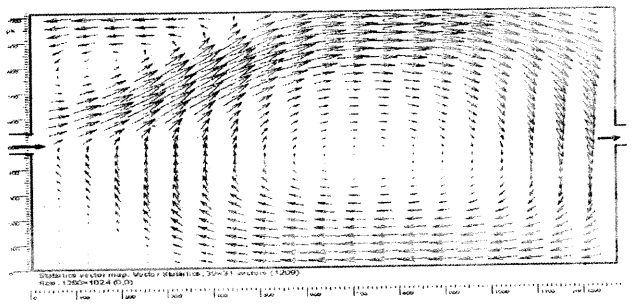

(e) clear water

Fig. 9. Flow pattern at different run times during test series 3.

two typical features were observed. The first was development of sediment deposition with ripples formation concentrated on the right hand side and along the center line later on; the second was concentrated on both right and left sides and very low in the core of the basin. In the following sub sections the results will be described with further details.

Fig. 10 presents the final bed elevations after 4.5 hours of testing of series 1. The mixture of water and sediment is advected and diffused throughout the basin following the general flow patterns described above. The footprint of the flow patterns was clearly visible in the morphology as shown in fig. 10-a. The resistance to flow is relatively small for the smooth and plane bed at the start. However, the flow resistance increases as ripples are being formed. The ripples play an important role in the interaction between the boundary layer flow structures and sediment transport.

Fig. 10-b shows the processed 3D surface bed elevation for the test series 1 after 4.5 hours. The asymmetric ripple patterns near the right side wall follow the same direction as the flow pattern shown in fig. 7. Ripples characteristics were measured manually before cleaning the basin. Moreover, several reference points were taken manually for calibration comparison with the UWS measurements. It was found that the UWS measures with a high accuracy of ±1mm and it's similar for the manual measurements. Nevertheless, some anomalous spikes are observed in fig. (10-b and 10-c) presents the contours for the sediment thickness layer. It can be easily seen that most of the sediment depositions has take place around the centerline and the downstream part. It may be concluded that a stable morphology has been reached after 4.5 hours whereas possibly a longer run would needed to confirm the question of full morphological equilibrium in the basin.

The sediment concentration and sediment depositions are highest along the centerline of the basin and reduce towards the sides as shown in figs. 10 and 11. Fig. 11 shows the evolution of the sediment depositions for the test series 2 (repeated test). The figure shows an almost similar sediment deposition pattern as was found for the series 1 presented in fig. 10.

There is a complex relation between flow patterns, sediment exchanges and sediment transport as well. Fig. 12 shows the results for the series 3 obtained after 4.5 hours of test run. Fig. 12-a presents a picture of the final bed evolution. It is noticed that the sediment deposition takes place in accordance with the flow patterns of figs. 9-a and 9-d. In the beginning it starts to form ripples near the right side wall leaving the area in the upstream corner void, which is associated with action of the small gyre.

From fig. 12-b it is clearly seen that the deposition at both upstream corners is very small. Most of the sediment deposits right below the main streamlines connected to the inflow channel. After the flow pattern has changed to the clockwise gyre, a symmetric ripple pattern formed near the left side wall, similar to the one at the right side which formed in the beginning. After a certain period of testing, the deposition on the left side gradually increased generating a wider bed elevation underneath the jet centerline with a width of approximately three times the inlet channel. Similarly, in the first few hours of the experiment the elevated bed has reached the right side wall and followed the course of the streamlines down to the outlet channel. It is remarkable that in the downstream part of the basin the bed is elevated on a rather narrow ridge. Fig. 12-c shows the contours for the sediment layer thickness. Here the relatively steep gradients near the inlet channel and the first part of the jet are clearly visible. It is quite likely that on a much larger time scale the relatively quiet zone in the upstream corners and the central part of the main gyre will eventually be filled up with the finest sediment fraction.

The final bed morphology obtained from test series 2 was used as the initial topography for a clear water test. Here, clear water without sediment was introduced into the basin to investigate the further bed evolution under those circumstances. Fig. 13 present the final bed deformation after 6 hours of clear water test. The most important change was found in the erosion of the bed near the entrance. No significant change has been observed anymore between the respective bed profiles after that period. Hence, for these flow

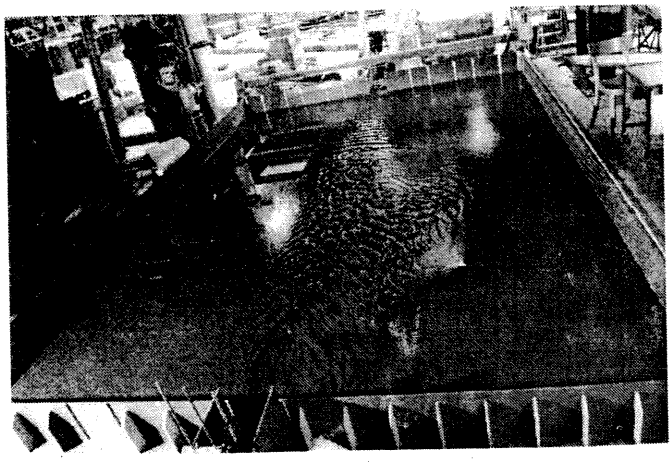

(a) Final bed features, photo looking downstream

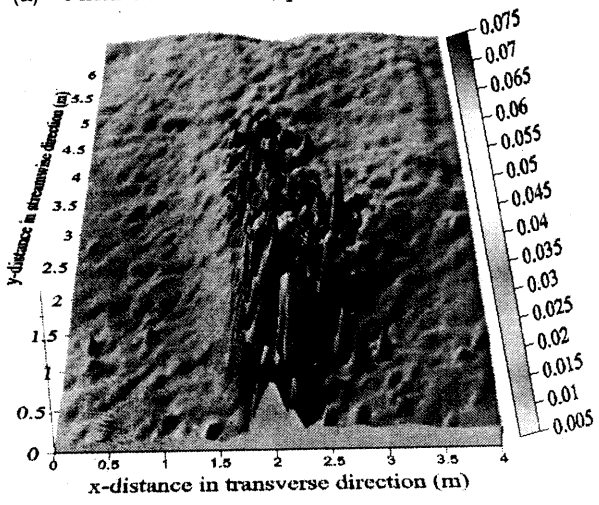

(b) 3-D surface of final sediment thickness layer

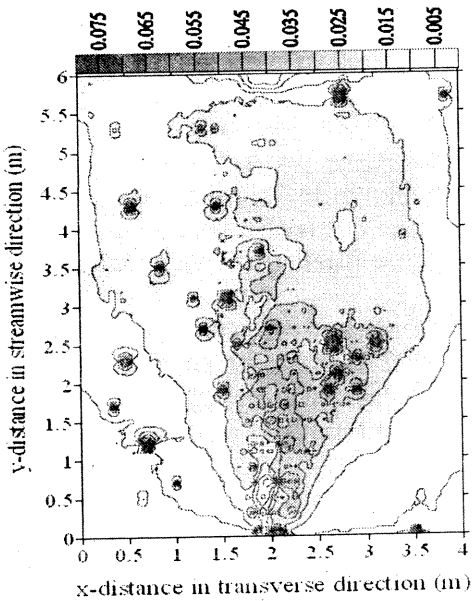

(c) Depositions contours

Fig. 10. Morphological results after 4.5 hrs of sediment supply for series 1.

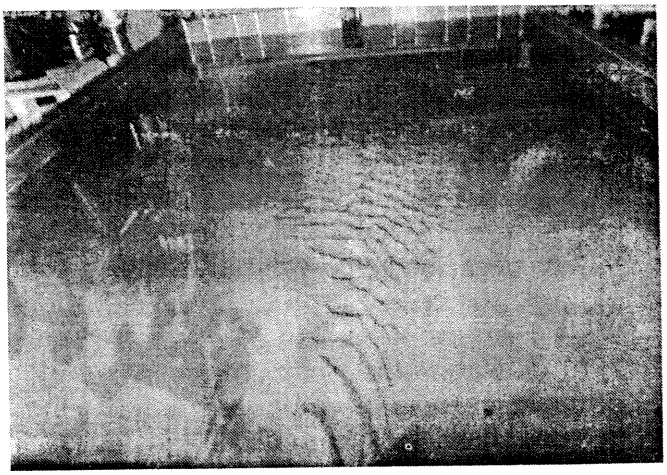

(a) Final bed features, photo looking downstream

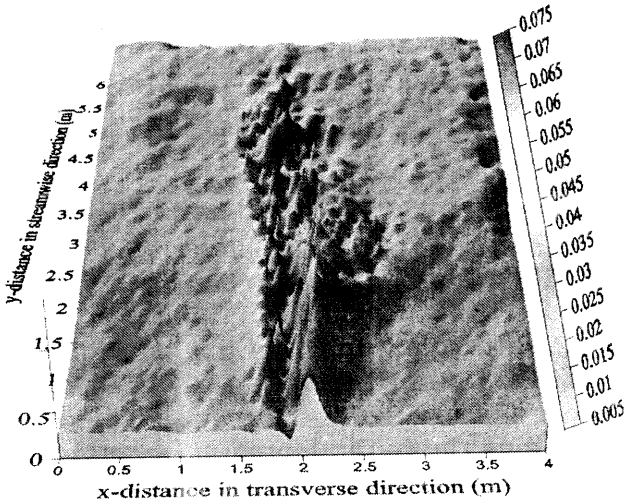

(b) 3-D surface of final sediment thickness layer

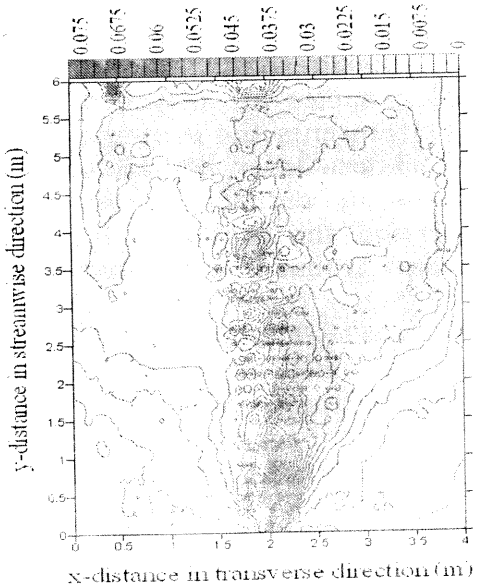

(c) Depositions contours

Fig. 11. Morphological results after 4.5 hrs of sediment supply for series 2.

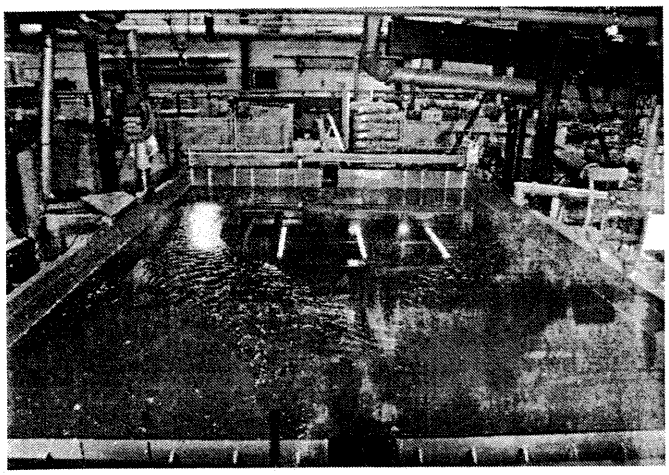

(a) Final bed features, photo looking downstream

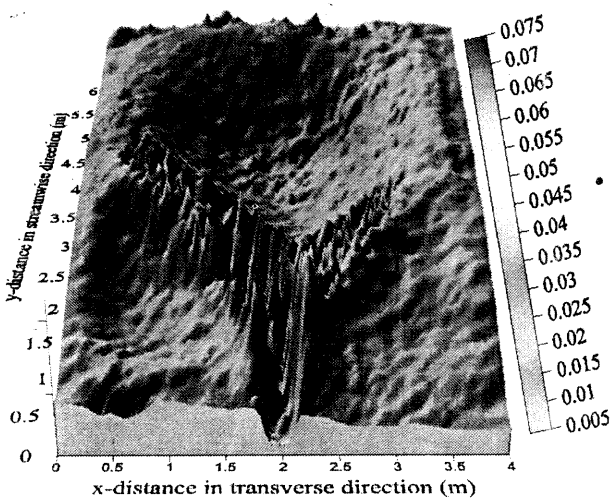

(b) 3-D surface of final sediment thickness layer

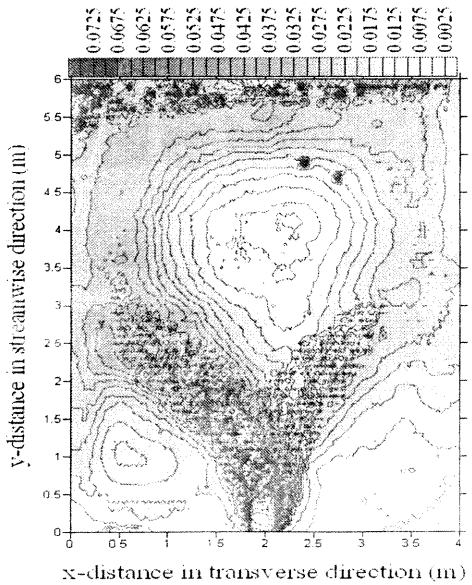

(c) Depositions contours

Fig. 12. Morphological results after 4.5 hrs of sediment supply for series 3.

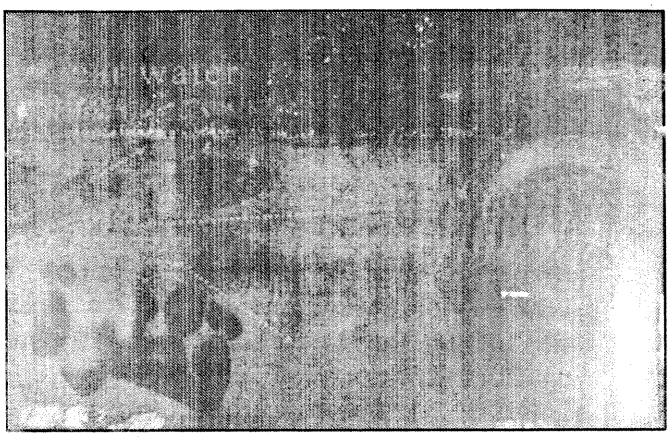

Fig. 13. Plan view for the test series 2 with the clear water inflow without sediment.

and sediment conditions, the bed might be considered as stable.

4. Conclusions

The first results of ongoing research on the influence of the geometry of a shallow reservoir on suspended sediment transport and deposition have been presented. The mechanism of sediment transport and deposition in the basin differs according to the test procedure. In the discontinuous feeding procedure, the gradual changes during the transitional state are missing due to the effect of stopping and restarting the flow. For the continuous feeding procedure, it was easy to reach a stable flow and bed form in the basin after 4.5 hours. Whether this represents a long-term equilibrium morphology will be checked by subsequent tests. It was found that the flow and sediment patterns are quite sensitive to the boundary and initial conditions. Although it is clear that an asymmetric flow pattern is favored, a symmetric pattern can persist for quite a long time. The experiment also shows the mutual interaction between flow and bed forms and the substantial increase in complexity when sediment transport and morphodynamics play a role.

Regarding the continuation of this research project the major goal is to find out which reservoir geometry leads to minimum sediment deposition. This requires experiments of long duration combined with numerical modeling techniques that include the processes as observed in this study.

References

[1] R.J. Adrian, "Particle-Imaging Techniques for Experimental Fluid Mechanics", Annu. Re. Fluid Mech., Vol. 23, pp. 261-304 (1991).

[2] R. Emttea, I. Fujita, M. Muste and A. Krufer, "Particle Image Velocimetry for Whole Field Measurement of Ice Velocities", Cold Regions Science and Technology, Vol. 26, pp. 97-112 (1997).

[3] I. Fujita, M. Muste and A. Kruger, "Large scale Particle Image Velocimetry for Flow Analysis in Hydraulic Engineering Applications", Journal of Hydraulic Research, Vol. 36 (3), pp. 397-414 (1998).

[4] S.A. Kantoush, E.F.R. Bollaert, J.L. Boillat, and A.J. Schleiss, Suspended Load Transport in Shallow Reservoirs", Final Proc. XXXI IAHR Congress. Korea Water Resources Association, Seoul, South Korea, pp. 1787-1799 (2005).

[5] H. Kobus, Hydraulic Modeling. Pitman, Boston, Mass. (1980).

[6] W. Mertens, "Model Tests for Sedimentation Process in Reservoirs", In W. Bechteler (cd.). Proceedings of EUROMECH 192, Munich, Neubiberg (1985).

[7] Metflow, UVP Monitor Model UVP-DUO-Users Guide. July 2002, Metflow SA, Lausanne, Switzerland (2002).

[8] C.J. Sloff, H.R.A. Jagers, and Y. Kitamura, "Study on the Channel Development in A Wide Reservoir", Proc. River Flow, Napoli, Italy, pp. 811-819 (2004).

[9] V. Weitbrecht, G. Kühn and G.H. Jirka, "Large Scale PIV-Measurements at the Surface of Shallow Water Flows", Flow Meas. and Instr. Vol. 13, pp. 237-245 (2002).

[10] M.S. Yalin, Theory of Hydraulic Models, London, Macmillan (1970).

Received June 30, 2007
Accepted June 7, 2008